2014

R32 Heat Transfer Coefficient During Condensation In A Mini-Channel Multiport Tube

Alejandro Lopez-Belchi
Technical University of Cartagena, Spain, alejandro.lopez@upct.es

Fernando Illán-Gómez
Technical University of Cartagena, Spain, fernando.illa@upct.es

José-Ramón García-Cascales
Technical University of Cartagena, Spain, jr.garcia@upct.es

Francisco Vera-García
Technical University of Cartagena, Spain, francisco.vera@upct.es

R32 Heat Transfer Coefficient During Condensation In A Mini-Channel Multiport Tube

Alejandro López Belchí, Fernando Illán Gómez, José Ramón García Cascales, Francisco Vera García

Technical University of Cartagena. Thermal and Fluids Engineering,
Cartagena, Murcia, Spain
C/ Doctor Fleming s/n. 30202. Cartagena – Murcia – Spain. alejandro.lopez@upct.es

ABSTRACT

The use of micro- and mini-channels in heat exchanger has increased in recent decades. They contribute to increasing efficiency and to reducing refrigerant charge and compactness of heat exchangers. The aim of this study is to experimentally determine heat transfer coefficient in mini-channels two-phase flow processes with the low GWP refrigerant R32 and compare it with the values provided by some of the correlations encountered in the existing literature.
In the existing literature there are a few publications studying the refrigerant R32. R32 has medium flammability, classified as A2 by ASHRAE. European air conditioning manufactures point to use R32 instead of R410A. R32 has lower global warming potential (GWP = 675) than R410a (GWP = 2088). Environmental improvements must be also considered. R32 is a single component refrigerant so recycling is easier than R410A process; also R32 is safer than R410A by NFPA 704 classification; with R410A a breathing apparatus is required in case of accident. On the other hand, R410A flammability is lower than R32 because of the addition of R125.
An installation for the study of condensation processes has been constructed at the "Technical University of Cartagena", Spain. The more relevant results of heat transfer coefficient will be presented in this paper. The analysed data have been measured for R32 flowing through aluminium square multiport tubes with a hydraulic diameter of 1.16 mm and compared with R410A. The influence of saturation temperature (or pressure), flow velocity, and vapour quality in heat transfer coefficient and frictional pressure gradient have been studied. The values considered for these variables are: saturation pressure corresponding to 30, 35, 40, 45, and 50ºC; flow velocities from 100 to 800 kg/(s·m^2); vapour quality from 0.05 to 0.9.

1. INTRODUCTION

Due to the ozone depletion potential associated to the use of CFCs and HCFCs refrigerants, charge reduction has become one of the most important issues to be considered in the design of a refrigeration system since the signing of the Montreal protocol in 1987. Although nowadays the use of CFCs and HCFCs is banned in most countries, charge reduction remains as an important issue due to the problems associated to the possible alternatives. The charge of HFC refrigerants must be minimized because of their great contribution to the direct greenhouse effect whereas in the case of natural refrigerants such as hydrocarbons and ammonia the problem is normally related to safety reasons (Poggi et al., 2008).
In the early 1980s, Tuckerman and Pease (1981) found that by reducing the tube diameter the heat transfer coefficient can be enhanced. Since then, mini and micro-channel technology has intensively researched as a way to reduce refrigerant charge while increasing the thermal performance of heat exchangers.
Since condensers contain the greater amount of refrigerant charge apart from the liquid lines, condensers utilizing mini or micro-channels are especially suited for charge reduction proposes. The design of high performance mini-channel condensers requires accurate predictive tools for both pressure drop and condensation heat transfer coefficient. For this reason, there are many international researchers working in two-phase flow heat transfer and pressure drop characterization during condensation in mini-channels, such as Del Col (2010), Bandhauer et al. (2006), Agarwal et al. (2008, 2010) or Park et al. (2011).
The use of low global warming potential (GWP) refrigerants combined to the mini-channel technology should allow improving the performance of refrigeration systems. The main goal of this study is to analyze two-phase flow pressure drop and heat transfer coefficient inside mini-channels during condensation of a low GWP refrigerant R32 and compare the results with its conventional alternative R410A.

2. EXPERIMENTAL APPARATUS

An experimental installation for the study of condensation processes inside tubes has been constructed at the Technical University of Cartagena, Spain.
The test rig used is depicted in Fig. 1. It consists of the primary (refrigerant) loop and three auxiliary loops: two cooling water loops and one hot water loop. Only the primary loop has been illustrated in Fig. 1.
The sub cooled refrigerant from the condenser *(1)* flows into a tank *(2)*. There is a controlled gear pump *(3)* connected to this tank, magnetically coupled to its variable speed electric motor.
When operating the installation for condensation measurements, the fluid is pumped through the Coriolis-effect mass flow meter *(4)* and the evaporator *(5)* where the refrigerant is vaporised up to a desired vapour quality. The previously mentioned Coriolis-effect flow meter also allows having refrigerant density and mass flow rate readings.
After passing through the evaporator, the two-phase mixture flows through a 100 mm copper tube to the inlet header *(6)*. Assuming a usual approximation (Agarwal et al., 2010; Zhang and Webb, 2001; Koyama et al., 2003; Sakamatapan et al., 2013) uniform two-phase flow is considered to be developed in the copper section before entering to the measuring section through the inlet header.
In the test section *(7)* the refrigerant is partly condensed with variation of vapour quality in all tests lower than 0.08. The fluid exits the test section through the outlet header *(8)* and then enters the condenser *(1);* the same cycle is repeated.
Two thermal baths are used in the condensation test: the first one provides the hot water used in the evaporator heated by Joule effect; the second one feeds the measuring section and the condenser after the test section. The temperature of these two circuits can be set to different values thanks to two mixing valves.
The test section inlet pressure is controlled by energy removal in the condenser. The main tank is a two-phase reservoir and vapour phase pressure is used to control the system pressure. The amount of refrigerant charge is enough to avoid vapour phase to be suctioned by the pump. A control system guarantees steady state conditions and ensures that measurements are properly made.
The pressure measurements are obtained through two digital pressure transducers, an absolute pressure sensor *(PT)* connected to the pressure port machined in the inlet header and a differential pressure sensor *(Dp)* connected to the outlet header. The range of absolute pressure transducer was fixed between 14 and 40 bars for both fluids. The differential pressure sensor range was fixed from 0 to 1 bar. The uncertainty is lower than 0.009 % for the differential sensor and 0.008 % for both absolute sensors. The entire accuracy must take into account the accuracy of the datalogger used to record intensity measurements of sensors.

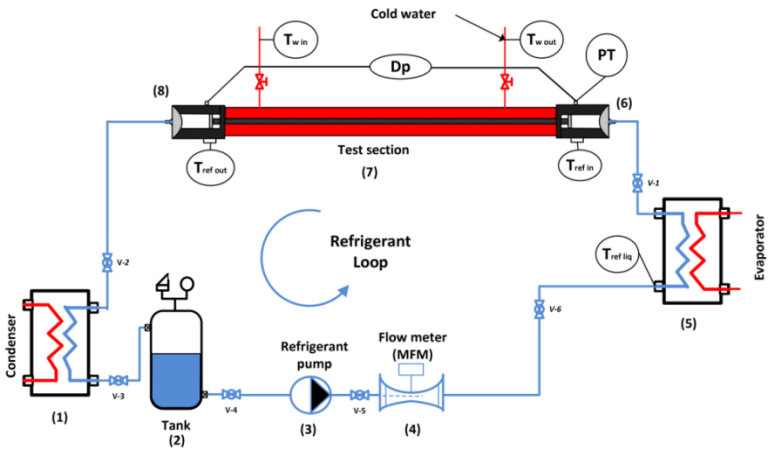

Figure 1: Experimental test rig.

2.1 Test section

The test section is made with a 1.16 mm hydraulic diameter multiport mini-channel tube brazed to two headers with a condensation measuring section of 259 mm length. The measuring section has an external casing so it is shaped as a counter-current heat exchanger with the cooling water flowing outside and the condensing fluid inside the mini-channel. Nine equally spaced thermocouples are soldered to the external tube wall to read wall temperature profile as shown in Fig 2.a. Refrigerant conditions are measured at the inlet and outlet test sections. The presence of both,

temperature and pressure sensors, at the inlet and outlet of the measuring sector allows a double check of the saturation conditions. Water case, tube dimensions and thermocouple measurement point detail can be seen in Fig. 2.b.

The geometry of the test section was measured with an optical microscope getting accurate values of inner areas, outer areas and perimeters. Surface roughness was measured with a Scanning Electron Microscope (SEM) at the Research Technology Support Service Building of the Technical University of Cartagena.

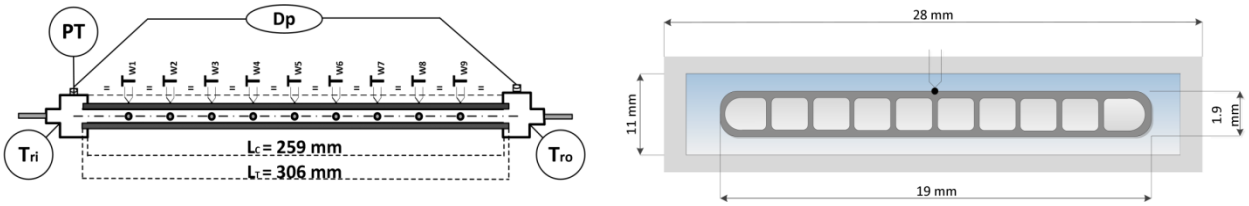

Figure 2: a) Test section sketch. b) Water case and thermocouple detail.

2.2 Experimental conditions

Experimental test conditions are summarised in Table 1. The ranges of mass velocities, saturation temperatures, maximum inlet vapour quality, and minimum outlet vapour quality and vapour quality change values are reported. The experimental tests were made with average vapour quality decreasing from 0.9 to 0.1 in maximum steps of 0.08.

Table 1: Experimental conditions

Fluid	G_{ref} (kg/m^{2}s)	Saturation Temperature (ºC)	Tests	Max X_{in}	Min X_{in}	dX
R32	350 to 800	20 to 55	158	0.94	0.13	<0.08
R410A	350 to 800	20 to 55	221	0.95	0.11	<0.08

3. DATA REDUCTION

3.1 Single-phase tests

In order to validate the experimental setup and to obtain the HTC value in water side, a series of single-phase tests were performed following the method developed by Park et al. (2011). Average single-phase Nusselt number for the refrigerant flow can be obtained as:

$$\overline{Nu}_{ref} = \frac{\dot{q}D}{k_{ref}(\bar{T}_{ref} - \bar{T}_{wall\ inner})} \quad (1)$$

Where:

$$\dot{q} = \frac{\dot{m}_w\ Cp_w(T_{w\ out} - T_{w\ in})}{A} = \frac{\dot{m}_{ref}\ Cp_{ref}(T_{ref\ out} - T_{ref\ in})}{A} \quad (2)$$

$$\bar{T}_{wall\ inner} = \bar{T}_{wall\ outer} - \frac{\dot{q} \cdot t}{k_{Al}} \quad (3)$$

$$\bar{T}_{wall\ outer} = \frac{1}{9}\sum_{i=1}^{9} T_{wall\ outer_i} \quad (4)$$

If refrigerant Nusselt number is calculated as explained above and compared with classical correlations such as Gnielinski, the results depicted in Fig. 3a are obtained.

Since during single-phase tests the fluid properties do not change appreciably along the tube, Reynolds number was considered practically constant and the local Nusselt number of the refrigerant flow is also expected to follow the Gnielinski correlation for turbulent flow:

$$Nu_{ref} = \frac{f/8\,(Re - 1000)Pr}{1 + 12.7\sqrt{f/8}\,(Pr^{2/3} - 1)} \tag{5}$$

The friction factor in turbulent region is obtained by means of eq. (6), that was verified to be the most accurate single-phase friction factor equation flow in smooth tubes by Fang et al (2011, 2012) and Brkic (2011).

$$f = 0.25\left[log\left(\frac{150.39}{Re^{0.98865}} - \frac{152.66}{Re}\right)\right]^{-2} \quad for\ Re \geq 3000 \tag{6}$$

Taking into consideration the previous explanation, the local heat flux in each position "*j*" was calculated from wall temperature measurements and refrigerant temperature calculation using eq. (7):

$$\dot{q}_{ref,j} = Nu_{ref,j}\,\frac{k_{ref,j}}{D_h}\left(T_{ref,j} - T_{wall\ inner,j}\right) \tag{7}$$

Refrigerant temperature in each position *"j"* was obtained from the temperature in the position *"j-1"* using eq. (8):

$$T_{ref,j} = T_{ref,j-1} - \left(\frac{\dot{q}_{ref,j-1} + \dot{q}_{ref,j}}{2\dot{m}_{ref}\,Cp_{ref}}\right) \tag{8}$$

For the first position eq. (8) becomes:

$$T_{ref,1} = T_{ref,in} - \frac{\dot{q}_{ref,1}}{\dot{m}_{ref}\,Cp_{ref}} \tag{9}$$

Since fluid properties depend on fluid temperature, the process is iterative and starts assuming linear evolution of refrigerant temperature, converging quickly to differences between two successive iterations lower than 0.5 %. Fig.3b shows local heat flux profile computed from single-phase experiments using eq. (7-9).

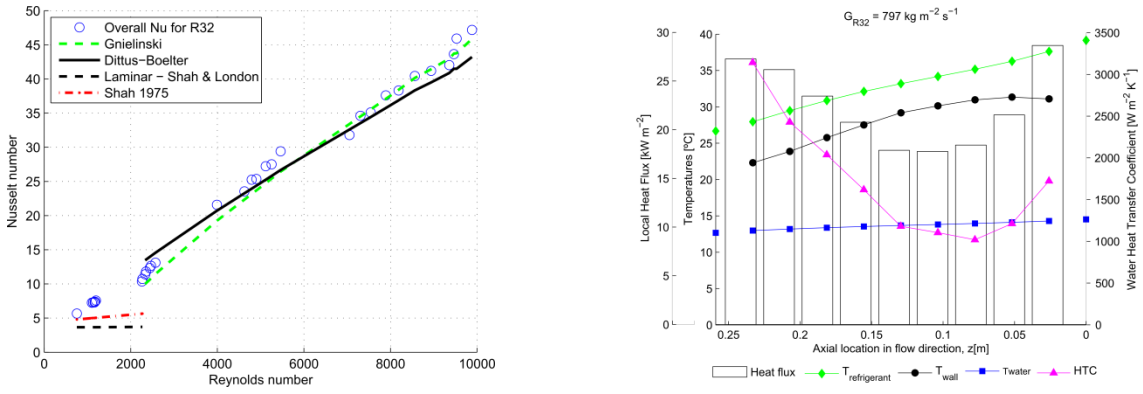

Figure 3: a) Liquid Nusselt number of R32. b) Obtained water side local parameters.

Once the local heat flux was calculated, a similar procedure was followed to obtain local HTC profile for the cooling water. Since all tests were carried out under steady-state conditions, there were no effects of energy accumulation in the tube walls and therefore the amount of heat flowing from the refrigerant to the inner wall must equals the heat flowing from the outer wall to the cooling water:

$$\dot{q}_{ref,j} = \dot{q}_{w,j} \tag{10}$$

$$T_{w,j} = T_{w,j-1} + \left(\frac{\dot{q}_{w,j-1} + \dot{q}_{w,j}}{2\dot{m}_w\, Cp_w}\right) \tag{11}$$

Since water properties depend on its temperature, water temperature profile was obtained from eq. (11) using an iterative process that begins assuming linear evolution of water temperature and quickly converges to differences between two successive iterations lower than 0.5 %.
Once the water temperature profile was obtained, the HTC profile of the cooling water was easily obtained applying eq. (12):

$$HTC_{w,j} = \frac{\dot{q}_{w,j}}{\left(T_{wall\ outer,j} - T_{w,j}\right)} \tag{12}$$

Fig. 3b shows the results obtained for the local HTC of the water following this procedure. According to this figure, a clear increase in the local heat flux was recorded at the inlet and the outlet of the test section.
From the refrigerant side point of view, the HTC remains nearly constant and the increase in heat flow can be explained by the increase in the temperature difference between refrigerant and tube wall recorded at the inlet and the outlet of the test section. From the water side point of view, the temperature difference between water and tube wall is lower at the inlet and the outlet sections of the water jacket, but this effect is compensated by the increase in water HTC recorded. This can be explained by the impinging effects at the inlet and the acceleration effects at the outlet sections of the water casing.
Several tests were made at different temperature levels with similar results and therefore it can be concluded that: the local Nusselt number of the water at each location is the same regardless of the Reynolds number of the refrigerant flow or its saturation temperature when the water maintains the same flow condition or Reynolds number. Fig. 4 shows several water HTC profiles obtained at different refrigerant saturation temperatures and mass flow rates. Only at low refrigerant Reynolds number the profiles obtained show a slightly different behaviour and have not been plotted in this figure. The blue line shows its average value.

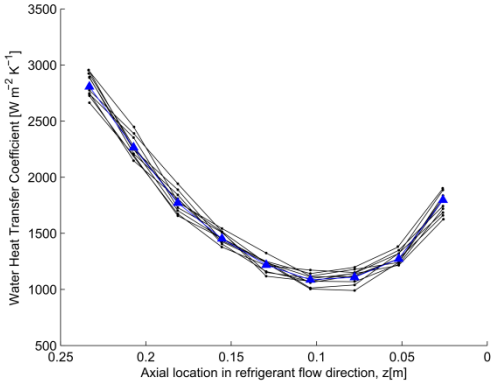

Figure 4: Water heat transfer coefficient profile at different refrigerant flow conditions.

3.2 Two-phase Heat Transfer Coefficient and pressure drop evaluation

Two-phase frictional pressure gradient is calculated by subtracting acceleration and accessories pressure drops to measured experimental pressure gradient, following the procedure described by López-Belchí et al. (2014).
Since single-phase tests were designed so that the total heat flow is quite similar to the value of the total heat flow in two-phase flow and single-phase test results have proved that the water HTC is almost independent of refrigerant conditions; it was assumed that the HTC of water side in refrigerant two-phase flow tests is similar to the HTC registered in turbulent single-phase tests.
The refrigerant local heat transfer coefficient $HTC_{ref,j}$ of each thermocouple location was determined by calculating the ratio of the heat flux $\dot{q}_j$ to the temperature difference between saturation temperature $T_{ref,j}$ and inner wall temperature $T_{wall\ inner}$ as follows:

$$HTC_{ref,j} = \frac{\dot{q}_j}{T_{ref,j} - (T_{wall\ inner})_j} \quad (13)$$

The heat flux $\dot{q}_j$ and water temperature at each thermocouple location were determined from the imposed water HTC profile obtained in single-phase tests, solving the two equations system formed by eq. (11) and eq. (14):

$$\dot{q}_{w,j} = HTC_{w,j}\left(T_{w,j} - T_{wall\ outer,j}\right) \quad (14)$$

Where, similarly to the procedure followed in single-phase tests, since water properties depend on its temperature, the water temperature at each point location, $T_{w,j}$, was calculated by an iterative process that begins assuming linear evolution of water temperature and quickly converges to differences between two successive iterations lower than 0.5 %.

The inner wall temperature $T_{wall\ inner}$ of the multi-port tube was derived from the measured outer wall temperature $T_{wall\ outer}$ and the heat flux:

$$(T_{wall\ inner})_j = (T_{wall\ outer})_j - \frac{\dot{q}_j \cdot t}{k_{Al}} \quad (15)$$

The refrigerant temperature at each thermocouple location, $T_{ref,j}$, was calculated from the corresponding saturation pressure, assuming saturated state. Small pressure drop values were recorded between the inlet and the outlet of the test section. A new correlation for frictional pressure drop prediction was developed in order to calculate saturation conditions on each thermocouple location.

Uncertainty for each parameter was calculated following the rules reported by Taylor (2009). Table 2 summarizes the uncertainty obtained for the most important parameters analysed.

Table 2: Summary of total uncertainty analysis for the results.

Parameter	Heat flux	Vapour quality	HTC	Inlet pressure	Frictional dP
Total Uncertainty (%)	3.4 - 4.5	2.2 - 12.5	5.6 - 21.7	1.6 - 3.4	2.2 - 11.9

4. EXPERIMENTAL RESULTS

In order to check the correct predictions of momentum pressure drop considered in this study, diabatic and adiabatic two-phase flow tests were carried out under similar conditions. These tests were carried out with different vapour quality variations, lower than 0.2. The results showed that frictional pressure drop predictions were similar in diabatic and adiabatic tests, so the expression for momentum pressure drop was precise for our tests.

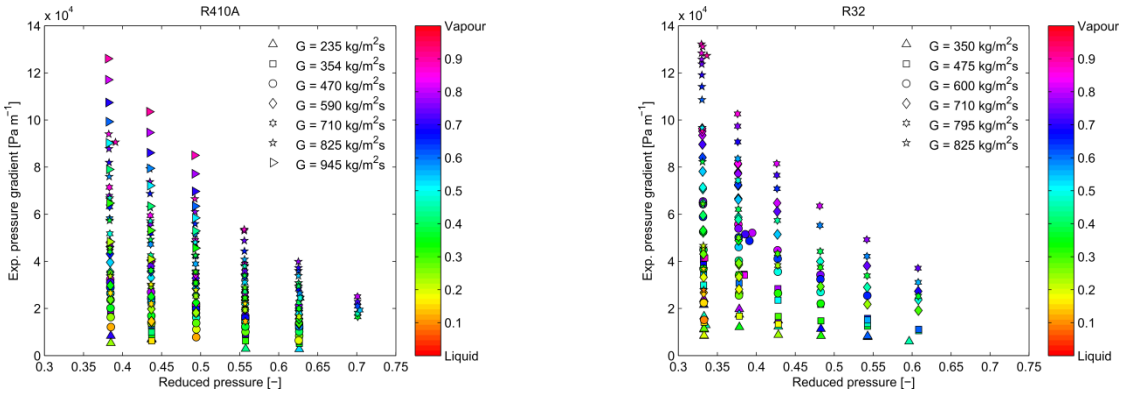

Figure 5: R410A and R32 frictional pressure gradients.

Frictional pressure gradients are plotted versus reduced pressure for different mass fluxes, and vapour qualities in Figure 5 for R32 and R410A. This figure represents reduced pressure in X axis and the frictional pressure drop in Y axis. Each marker is filler in grey colour, as clearer the marker is filled the higher vapour quality value it has.
According to the experimental results plotted in Figure 5, experimental values of two-phase frictional pressure gradient follow conventional theory. Frictional pressure drop increases with higher mass velocities and vapour quality values. Also, frictional pressure drop gradient values decrease with increasing values of reduced pressure.
A classical graph is also provided at a fixed saturation temperature of 40ºC in Figure 6. Pressure gradient is depicted versus vapour quality at three different mass velocities. According to the results plotted in this figure, R410A performs better than R32, since the pressure drop is up to a 25 % lower. This effect is clearer at higher mass velocities and lower saturation temperatures.

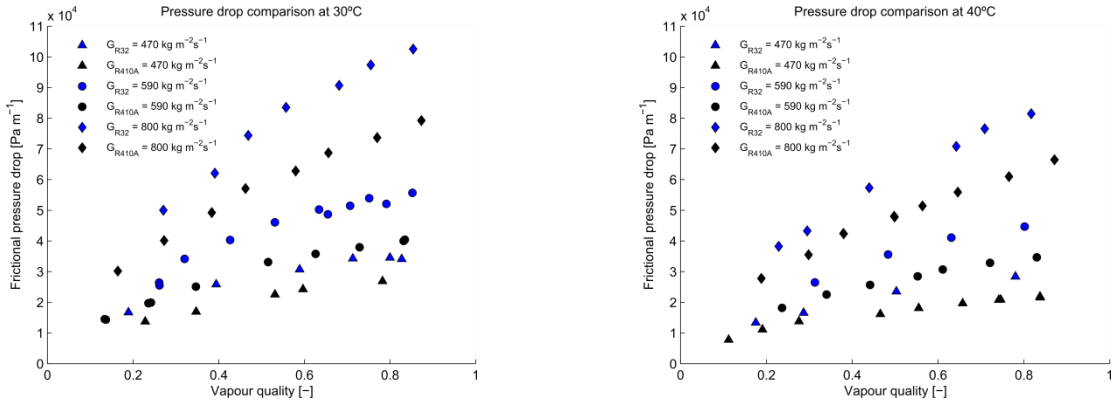

Figure 6: R410A and R32 frictional pressure gradients.

Heat transfer coefficients of both refrigerants were also experimentally measured along the dome at different saturation conditions. In all experimental tests the same behavior is repeated with small differences. In all tests the heat transfer coefficient of R32 is higher than R410A values. This difference is clearly lower as mass velocity increases and not so clear the saturation temperature effect, as depicted in Figure 7.

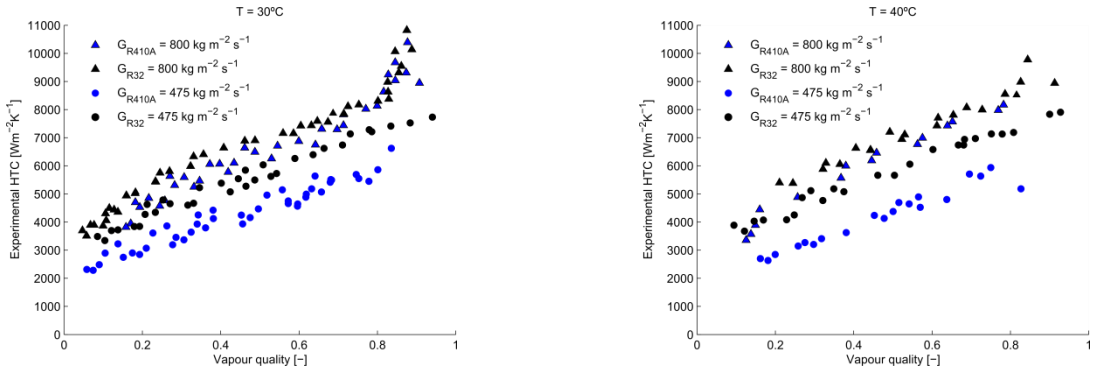

Figure 7: R410A and R32 heat transfer coefficients.

Table 3: Fluid properties at 30 & 40 ºC.

Refrigerant & Sat. T. [ºC]		Pressure [kPa]			Density [kg m^{-3}]		Viscosity [μPa s^{-1}]		Therm. Cond. [W mK^{-1}]	
		Critical	Saturation	Reduced [-]	Liquid	Vapour	Liquid	Vapour	Liquid	Vapour
R410A	30	4901.9	1889.8	0.385	1032.6	76.57	110.36	14.04	0.086	0.016
	40		2426.2	0.492	975.26	103.3	95.84	14.91	0.081	0.019
R32	30	5782.0	1928.0	0.333	939.58	54.79	107.22	13.12	0.122	0.016
	40		2478.9	0.428	892.98	73.29	94.97	13.83	0.115	0.018

The different behaviour obtained can be explained by the differences between both refrigerant properties detailed in Table 3. Since at 40 ºC both refrigerants have similar viscosity values, their Reynolds number and friction factor are very similar at a given mass velocity. Therefore the higher pressure drop is obtained with R32 that flows at a higher velocity because of its lower density. This effect is even clearer at 30 ºC because of the slightly higher differences between both fluid density and viscosity. On the other hand, R32 presents a higher liquid thermal conductivity that leads to better heat transfer properties. Since the thermal conductivity difference between both refrigerants is almost independent of the temperature, differences between both refrigerants seem to be independent of the saturation temperature as shown in Figure 7. These differences in fluid properties and their variation can also be explained by the differences in reduced pressure shown in Table 3.

5. MODELS COMPARISON

The experimental data recorded for these two fluids have also been compared with some models available in the open literature. The best predictions are provided by Koyama et al. (2003) model for both fluids.

Webb et al. model clearly overestimates heat transfer coefficient of R32 at all saturation pressures. On the other hand, the model developed by Koyama et al. is quite accurate and performs really well with R32, the predictions are a bit poorer with R410A but are still accurate.

Regarding to the prediction of frictional pressure gradient, several model predict frictional pressure gradient accurately. Some of the most accurate found are depicted below. In that case, the behavior of these models is quite similar in both predictions.

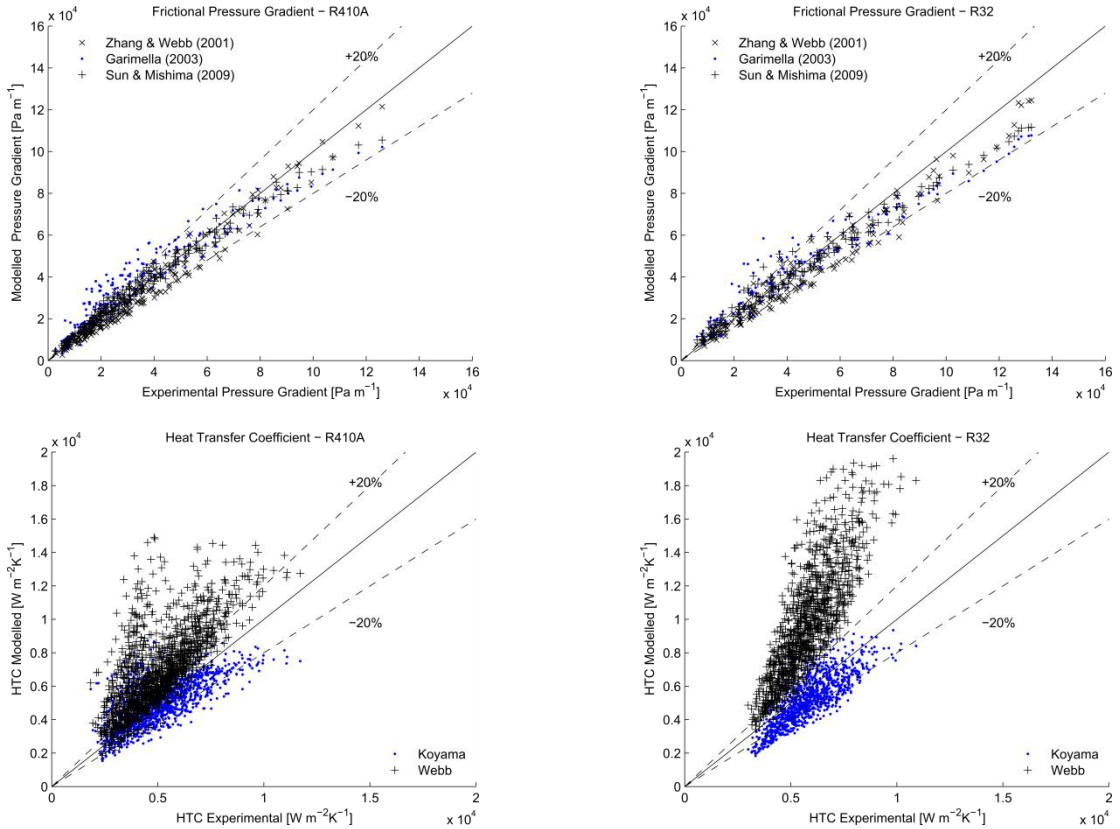

Figure 8: Experimentally measured pressure gradient and heat transfer coefficient for R410A and R32 compared with several models.

6. CONCLUSIONS

R32 and R410A pressure drop and heat transfer coefficient values recorded in a mini-channel multi-port tube during condensation processes have been reported. The descriptions of the installation and data reduction have also been defined.

R32 is a new refrigerant featuring excellent energy and environmental efficiency. The global warming potential of R32 is approximately 1/3 that of R410A. It is more efficient than R410A in around a 5 % in cooling and heating energy systems. This higher efficiency allows reducing refrigerant changer by 20 – 30 % in each air conditioner unit. Finally, R32 is a single component fluid so it can be recovered and recycled easily after use.

Some manufacturers are using R32 instead of R410A in domestic and industrial cooling units due to these advantages.

In addition to all of these advantages, the use of R32 in mini-channel equipment lead out to higher efficiencies but accurate predictive tools are required for pressure drop and heat transfer coefficient evaluation.

Not many models are able to predict reasonably well HTC of these two fluids; this may be explained because of the working pressure range of these fluids. Both of them are high pressure refrigerants and not many authors have experimentally measured them.

In this paper, the authors have presented the experimental data measured with both fluids and the differences found between them.

NOMENCLATURE

C_p	Specific heat	(J/(kg K))
D	Hydraulic diameter	(m)
f	Friction factor	(-)
G	Mass velocity	(kg/(m^2 s))
HTC	Heat Transfer Coefficient	(W/(m^2 K))
k	Thermal conductivity	(W/(m K))
$\dot{m}$	Mass flow rate	(kg/(m^2 s))
Nu	Nusselt number	(-)
Pr	Prandtl number	(-)
$\dot{q}$	Heat flux	(W/m^2)
Re	Reynolds number	(-)
t	Thickness	(m)
T	Temperature	(K)
X	Vapour quality	(-)

Subscript

ref	Refrigerant
w	Water
wall	Wall

ACKNOWLEDGEMENT

This study has been carried out within the framework of two research projects; one financed by the Spanish Ministry of Science and Innovation (ref: 08766/PI/08) and the other by the Spanish Ministry of Economy and Competitiveness (DPI2011-26771-C02-02).

REFERENCES

Agarwal, A., Garimella, S. Dec. 2008. Modeling of Pressure Drop During Condensation in Circular and Noncircular Microchannels, *J. Fluid Eng.- T. ASME* vol. 131, no. 1, p. 011302.

Agarwal, A., Bandhauer, T. M., Garimella S., Sept. 2010. Measurement and modeling of condensation heat transfer in non-circular microchannels, *Int. J. Refrig*., vol. 33, no. 6, pp. 1169-1179.

Bandhauer, T. M., Agarwal, A., Garimella, S. Mar. 2006. Measurement and Modeling of Condensation Heat Transfer Coefficients in Circular Microchannels. *J. of Heat Tran. - T. ASME*, vol. 128, no. 10, pp. 1050-1059

Brkic, D., Sept. 2011. New explicit correlations for turbulent flow friction factor. *Nucl. Eng. Des.*, vol. 241, no. 9, pp. 4055-4059.

Del Col, D., Torresin, D., Cavallini, A. Nov. 2010. Heat transfer and pressure drop during condensation of the low GWP refrigerant R1234yf. *Int. J. Refrig*., vol. 33, no. 7, pp. 1307-1318.

Fang, X., Xu, Y., Zhou, Z. Mar. 2011. New correlations of single-phase friction factor for turbulent pipe flow and evaluation of existing single-phase friction factor correlations. *Nucl. Eng. Des.*, vol. 241, no. 3, pp. 897-902.

Fang, X., Zhang, H., Xu, Y., Su, X. Jan. 2012. Evaluation of using two-phase frictional pressure drop correlations for normal gravity to microgravity and reduced gravity. *Adv. Space Res.*, vol. 49, no. 2, pp. 351-364.

Garimella, S., Killion, J.D., Coleman, J.W., 2003. An Expermentally Validated Model for Two-Phase Pressure Drop in the Intermittent Flow Regime for Noncircular Microchannels, *J. Fluids Eng.*, 125, pp. 887-894.

Koyama, S., Kuwahara, K., Nakashita, K., Yamamoto, K. June 2003. An experimental study on condensation of refrigerant R134a in a multi-port extruded tube. *Int. J. Refrig*., vol. 26, no. 4, pp. 425-432.

López-Belchí, A., Illán-Gómez, F., Vera-García, F., García-Cascales, J.R., 2014. Experimental condensing two-phase frictional pressure drop inside mini-channels. Comparisons and new model development. *Int. J. Heat Mass Transfer*., vol. 75, pp. 581–591

Park, J.E., Vakili-Farahani, F., Consolini, L., Thome, J.R., Apr. 2011. Experimental study on condensation heat transfer in vertical minichannels for new refrigerant R1234ze(E) versus R134a and R236fa," *Exp. Therm. Fluid Sci.*, vol. 35, no. 3, pp. 442-454.

Poggi, F., Macchi-Tejeda, H., Leducq, D., Bontemps, A. May 2008. Refrigerant charge in refrigerating systems and strategies of charge reduction," *Int. J. Refrig*., vol. 31, no. 3, pp. 353-370.

Sakamatapan, K., Kaew-On, J., Dalkilic, A. S., Mahian, O., Wongwises, S. Sept. 2003. Condensation heat transfer characteristics of R-134a flowing inside the multiport minichannels. *Int. J. Heat Mass Tran.*, vol. 64, no. 0, pp. 976-985.

Sun, L., Mishima, K. 2009. Evaluation analysis of prediction methods for two-phase flow pressure drop in mini-channels, *Int. J. Multiphase Flow*, 35, pp. 47–54

Taylor, B. N. 2009. *Guidelines for Evaluating and Expressing the Uncertainty of NIST Measurement Results (rev* DIANE Publishing.

Tuckerman, D.B., Pease, R. F. W. May 1981. High-performance heat sinking for VLSI," *Electron Device Letters, IEEE*, vol. 2, no. 5, pp. 126-129.

Webb, R.L. 1998. Prediction of condensation and evaporation in micro-fin and micro-channel tubes. In: S Kakac, AE Bergles, F Mayinger, H Yuncu, editors. Heat transfer enhancement of heat exchangers. Netherlands: Kluwer Academic Publishers; p. 529-550

Zhang, M., Webb, R.L. Oct. 2001. Correlation of two-phase friction for refrigerants in small-diameter tubes. *Exp. Therm. Fluid Sci.*, vol. 25, no. Issues 3-4, pp. 131-139.